NUMERICAL THERMAL ANALYSIS IN ELECTRON BEAM ADDITIVE MANUFACTURING WITH PREHEATING EFFECTS

Ninggang Shen, Kevin Chou

Department of Mechanical Engineering
The University of Alabama
Tuscaloosa, AL 35487, USA

Abstract

In an early study, a thermal model has been developed, using finite element simulations, to study the temperature field and response in the electron beam additive manufacturing (EBAM) process, with an ability to simulate single pass scanning only. In this study, an investigation was focused on the initial thermal conditions, redesigned to analyze a critical substrate thickness, above which the preheating temperature penetration will not be affected. Extended studies are also conducted on more complex process configurations, such as multi-layer raster scanning, which are close to actual operations, for more accurate representations of the transient thermal phenomenon.

Introduction

Titanium (Ti) alloys, e.g., Ti-6Al-4V, are materials with outstanding mechanical properties such as low density, high strengths, good chemical resistance and excellent biocompatibility. The combination of these characteristics has made Ti alloys attractive in many applications in medical, aerospace and automotive components. However, fabrications of parts made of Ti alloy by conventional manufacturing processes such as casting and forging are costly, inefficient, and environmentally hazardous. Moreover, the high melting point and chemical affinity at elevated temperatures cause the processing of Ti alloys very challenging [1].

In recent years, Additive Manufacturing (AM) using commercially available atomized metallic or alloyed powders with a high-energy heat source has been developed and applied to fabricate complex-shaped, multifunctional, or custom designed components. Various types of mechanical components can be built with such a layer-based fabrication technology through a computer controlled machine [2]. This provides the industry with an effective alternative solution for the processing of Ti alloy parts.

Electron Beam Additive Manufacturing (EBAM) is one of emerging AM technologies that are uniquely capable of making full density metallic components. Arcam AB [3] developed and commercialized EBAM machines, in which metallic powders are melted by a fast moving electron beam, then rapidly cooled and solidified; the detailed description of the process can be found in [2]. The electron beam technology can provide both a high power density and energy efficiency. In addition, material properties of EBAM parts are comparable to or even better than parts made by conventional means.

Despite many potential advantages over conventional processing technologies, sometime EBAM still encounters several process/part deficiencies [4], which may be due to lack of processing understanding. Hence, accurate physical models of both thermal and mechanical behaviors in EBAM are necessary to better investigate the process phenomena and part output in order to determine appropriate process parameters that are presumably correlated to the occurrence of the deficiencies.

However, the simulation of the thermal phenomenon in EBAM is still a challenging task because of the complex heat transport and heat intensity distribution, and the interactions among the thermal, mechanical, and metallurgical phenomena. Of one particular significance, powder sintering takes place in EBAM, called preheating, usually heated to about 700-800 °C, in the powder bed prior to the actual melting process. Further, the effect of sintering may be important, and thus, the preheating should be modeled as well as a part of the thermal cycle. In a previous work conducted by the authors [5], it has been shown that Finite Element (FE) analysis is an efficient way to conduct this kind of complex thermal-phenomenon analysis. An FE thermal model was developed by the authors using ABAQUS software to investigate the dynamic temperature and cooling rate distributions during EBAM. The model incorporated the temperature and porosity dependent thermal properties for the studied material, Ti-6Al-4V powders. The model has been applied to preliminarily study the EBAM process parameter effects, such as the beam speed. The electron-beam heat source was modeled as a conical volumetric body heat flux at the surface of the build part and the intensity is distributed as a Gaussian distribution horizontally and decays linearly along the penetration depth based on the review of the Electron Beam Welding (EBW) literature [6-8]. To account for the convection effect, the thermal conductivity in the molten pool was increased in the model, per Taylor et al. [9], De and DebRoy [10]. A user subroutine coded in FORTRAN was applied to consider the latent heat of fusion, to include temperature dependent and porosity dependent thermal properties of solid or powder materials, and to define the material state change. The porosity dependent thermal properties of powders were modeled based on the model from Sih and Barlow [11], and the model from Tolochko et al. [12], respectively. The results indicated that the powder porosity strongly affects the thermal characteristics such as the melt pool size and the cooling rate in the EBAM process.

The previous model in development is just a preliminary study of this subject matter – thermal modeling of EBAM. A few assumptions were made, but might not be appropriate in certain conditions, e.g., the definition of thermal initial conditions (ICs). In the previous model, the initial temperature of the whole model was set uniformly distributed, at 750 °C, before melting. This is deviated from the actual condition, since the preheating is also a transient process.

The objective of this study is to extend the developed thermal model and tested with more complex conditions that better represent the actual process, e.g., preheating to establish the thermal initial conditions of the part prior to the electron beam melting process and to attempt multiple layer, cross-raster scanning. The intent is to improve the model more close to the actual process, and to test the capability and flexibility of the model. Specifically, in this paper, an extended study is conducted to investigate the effect of the preheating process on the thermal initial conditions with the FE simulation of different substrate thicknesses. A preheating

temperature penetration is obtained and a critical substrate thickness is determined. Then, the FE thermal model is modified for further analysis of the new initial condition effects. With the modeled thermal initial conditions, a more complex thermal analysis is conducted to simulate a multi-layer cross-raster scanning. In the end, a case study of the powder porosity effect is evaluated with different configurations of the substrate materials used.

Preheating Process Investigation

In the earlier model constructed by the authors, the entire substrate was considered with a uniform temperature distribution of the assumed preheat temperature (e.g., assumed to be 750 °C). This obviously may not be a suitable assumption in some cases. Just like the melting step, the preheating stage itself is of transient nature as well. Thus, the result of the preheating process should be considered as thermal initial condition to more accurately model the thermal characteristics of the entire EBAM process. The FE model can be a very efficient way to examine the preheating effect on the transient thermal phenomena in EBAM.

In this phase of the investigation, an FE methodology to simulate the preheating stage has been implemented. The whole powder bed is 300×300 mm^2 at the top surface. Four levels of substrate thicknesses of the powder beds were considered in this study: 10, 70, 100, and 150 mm. To reduce the computational cost, the preheating area was fixed as 100×100 mm^2 at the top surface and located at the center of the powder bed. Some preheating parameters used in this study are shown in Table 1, which was reported by Gaytan et al. [2]. The start plate is generally heated to above 600 °C (assumed) before the building cycle. However, the temperature of the spread powders from the powder hopper is unknown. In this study, the initial powder temperature was assumed as 200 °C. Therefore, at the beginning of the simulation, the substrate temperature was set at 600 °C with the powder layer of an initial temperature of 200 °C in the FE thermal model. During the simulation, the temperatures at bottom of the substrate (start plate) were set at a uniform 600 °C (assumed) for all conditions.

Table 1. Parameters for Preheating Analysis.

Acceleration Voltage (kV)	Beam Current (mA)	Scan Speed (m/sec)	Initial Substrate Temperature (°C)	Initial Powder Temperature (°C)
150	30	15	600	200

Once the simulation starts, the electron beam, modeled as a conical volumetric intensity as described above [5], scans across the powder-layer surface as a moving source of heat. The heat source transverses in a raster pattern a few times until the powder layer temperature reaches the target value for powder sintering, which is set as 750 °C. The raster direction is consistent at the same layer. The material thermal properties of both the powder and bulk solid materials are the same as before and can be found in Shen and Chou [5]. Since the preheating phase is for powder sintering, no melting is to happen. Therefore, the material state transformation function in the code (from powder to solid) is not needed in this section of investigation. The final simulation results also indicated that the peak temperatures do not reach the melting point of Ti-6Al-4V, 1650 °C.

Figure 1 shows an example of the simulated temperature contour for the 150 mm thick substrate with a cut-off sectional view right after 28 times of scanning. It can be seen that the high temperature zone is generally confined in the top surface materials, i.e., the preheating temperature penetration is fairly shallow, and the temperature drops to close to 600 °C. Such a thermal phenomenon can be noted, similarly for all conditions with different substrate thicknesses. Figure 2 shows the simulated vertical temperature profile comparisons of all conditions. Two comparisons are made: one is the vertical temperature profiles within the whole substrate domain, labeled with (i) along the first row of plots; the other is the vertical temperature profiles within the top 10 mm, labeled with (ii) on the second row. The results of the 10 mm substrate case are only shown in the second comparison on the second row of the figure. All the profiles were obtained at the center of the preheating area. For each condition, four profiles after different repeated scans are shown in each chart. The purple solid line and blue dash-dotted line are the profiles after the final scan and the first scan, respectively. The other two profiles are selected after the intermediate scans in order to show the transition of temperature evolutions. It can be easily noted that preheating does not affect the domain beneath 10 mm depth too much (on the first row), and the target preheating temperature of 750 °C has a fairly constant penetration of 0.5 mm to all cases (on the second row). Therefore, the substrate thickness of 10 mm seems to be sufficient for the thermal analysis of the EBAM process and can be considered as the critical substrate thickness beyond which the preheating temperature penetration will not be affected. In addition, the preheating temperature penetrations are constantly to all conditions, regardless of the substrate thickness, roughly 0.5 mm which is equivalent to 5 powder layers. This can be considered as the guidance in improving the previous thermal model developed by the authors [5].
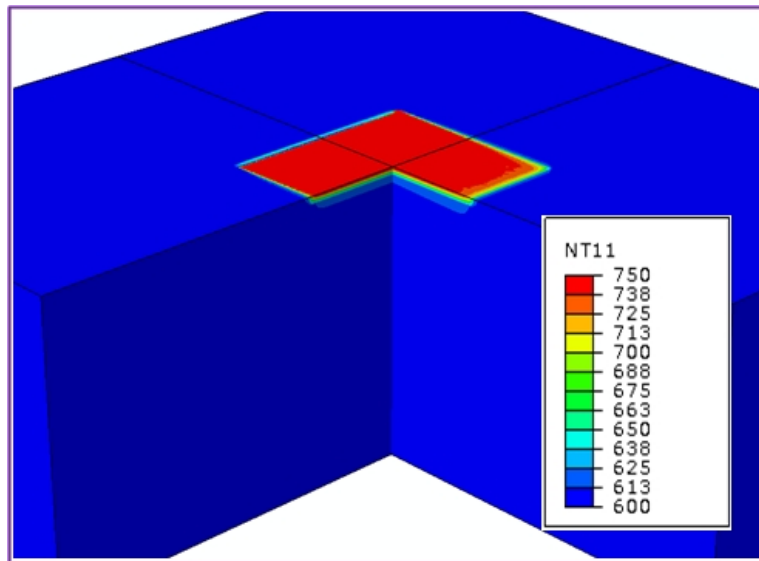

Figure 1. Temperature contour of the preheating simulation for 150 mm thick substrate at a cut-off cross-sectional view.
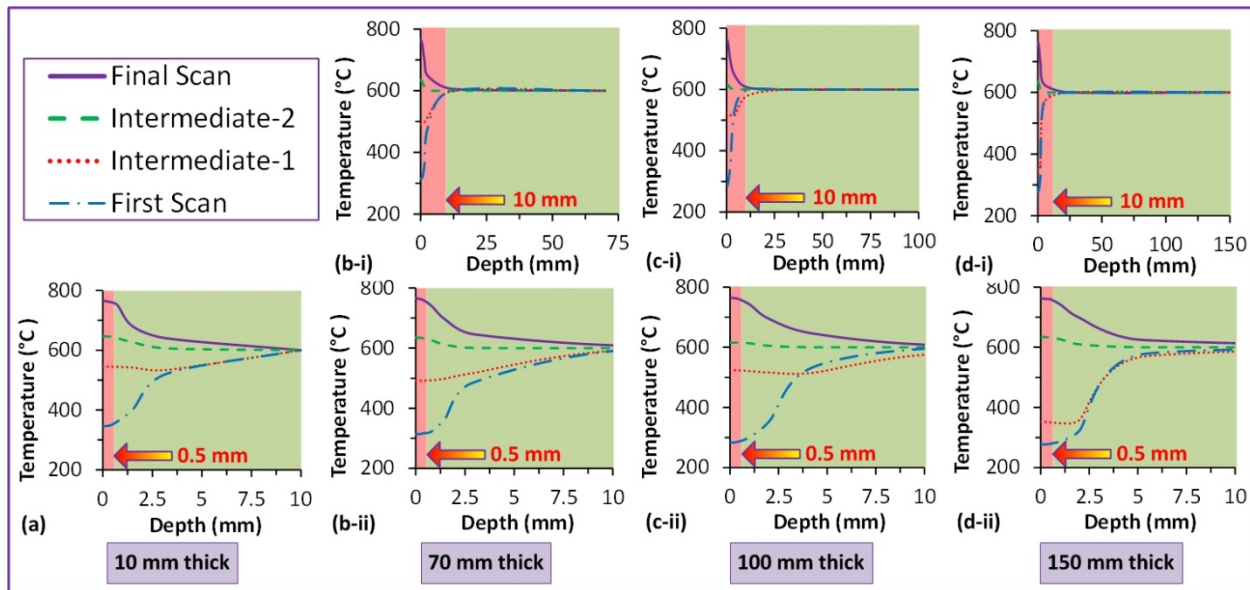
Figure 2. Simulated temperature profiles for various substrate thicknesses, (i): Temperature profile within the entire substrate, and (ii): Temperature profile within the 10 mm depth.

Modified Thermal Model

The FE thermal simulation was remodeled based on the conclusions obtained from the last section: the critical substrate thickness and the preheating temperature penetration depth. The substrate thickness was increased from 6 mm to 10 mm and the thermal initial conditions were redefined using the preheating process simulation. A particular domain is generated and within the top 0.5 mm, a uniform temperature of 750 °C was assigned as the preheating temperature penetration, then the temperature linearly decays along the depth from 750 °C to 600 °C. The results of the change is shown in Figure 3a, which is just before applying the electron beam heat source. The bottom of the substrate was still set at a constant temperature of 600 °C.

Two simulation cases of a single straight scan path were conducted to examine the effect of the new thermal initial conditions. One began with the new thermal initial conditions and the other used with the previous thermal initial conditions of a uniform temperature of 750 °C in the whole substrate. The simulation results are shown in Figure 3b and 3c for the new and previous thermal initial conditions, respectively. The simulated temperature contours share the same legends. With the application of the new thermal initial conditions, the peak temperature drops about 120 °C. It can be easily observed that the new thermal initial conditions lead to a smaller heat penetration (the green domain) than the results of the uniform thermal initial conditions. Although the overall melt pool did not change significantly, the melt pool size actually changed to some extent at the tail geometry. The new thermal initial conditions result in a sharper tail than the results of the old thermal initial conditions. Therefore, all the results above indicate that the modified thermal model may be significant to this numerical thermal analysis. This change will be implemented in future studies.
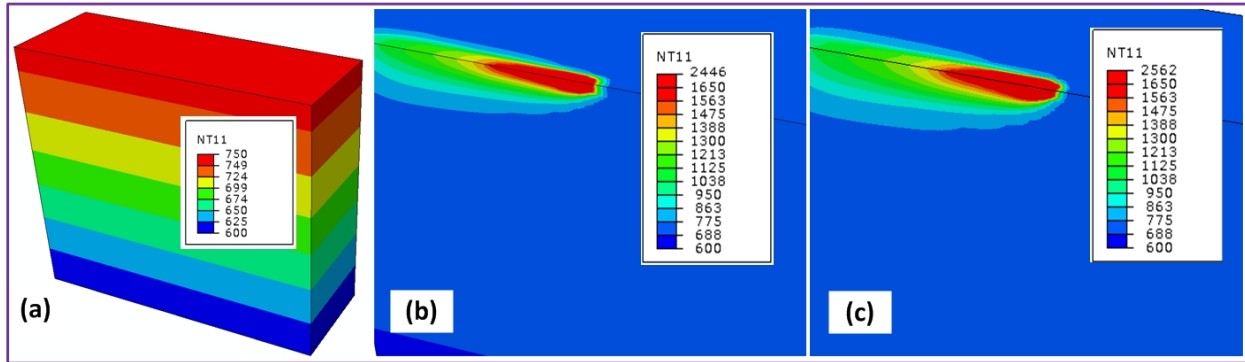
Figure 3. Applied new thermal initial conditions (ICs): (a) New thermal ICs, (b) Simulated temperature contour with new thermal ICs, and (c) Simulated temperature contour with old thermal ICs.

Multi-Layer Cross-Raster Scanning

With the modified model, the thermal analysis was advanced to a multi-layer cross-raster scan pattern. Although the significant effect of the electron beam melting can be illustrated with the simulation of a straight scan path, the cross-raster scan pattern better represents the actual heating cycles. In addition, it is necessary to consider a multi-layer building in order to fully investigate the repeated thermal process, as well as the residual stresses evolution in the future thermo-mechanical analysis. Zhang and Chou [13, 14] investigated the fused deposition modeling (FDM) process; the author developed a FE model including the heat and mass transfer phenomena coupled with mechanical displacement/deformation, and the phase changes to analyze the mechanical and thermal phenomena in FDM. The element activation function was applied to simulate the additive nature of the process. Further, the model was used to predict residual stresses and part distortions after multiple-layer depositions.

The FE thermal model utilized in this section generally has the similar configuration introduced by Shen and Chou [5]. The geometric domain of the model was divided into two sub-domains: a substrate and a powder layer. The thickness of the powder layer was assumed as 0.1 mm and the substrate thickness was set as 9.9 mm, with the total thickness of the model as 10 mm, which is roughly the critical thickness determined above. Two sequential layer-depositions were simulated and the cross-raster scan is shown in Figure 4. The area of the raster scan patterns was 3×3 mm^2 for each layer and the raster width was the same as the beam diameter (4 mm). After the melting phase of each layer, there was a hold of about 10 seconds between two sequential melt scans. Also, during the hold, a heat dissipation phase was simulated and the thermal initial conditions were applied again. For the material addition, the technique of element activations was applied. The second-layer of powders was modeled before the simulation execution, but was deactivated in the melting phase of the first layer. It was reactivated at the melting phase for the second layer. Then, the heating simulation resumed again from the same starting point with the alternative raster direction, but with the same raster width.
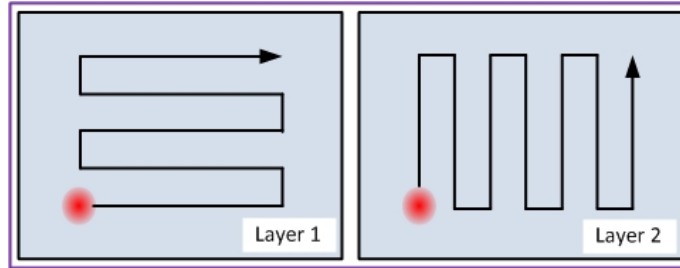
Figure 4. Schematic of the cross-raster scan pattern applied in the multi-layer EBAM thermal analysis.

There were two cases conducted in the multi-layer cross-raster scan pattern simulations. The two cases had different substrate material conditions; one had an entire solid substrate, but the other had a half-solid, half-powder substrate. In the first case (entire solid substrate), the substrate was considered as solid bulk materials which were solidified from the powders in the melting process of previous layers. The second case simulation (half-solid, half-powder substrate) represents a part model having overhang geometry, which is not uncommon. The simulation results of the two cases are discussed in the following sections.

Entire Solid Substrate

Based on the aforementioned study, the thermal initial conditions are supposed to be consistent in each layer. Furthermore, the simulated raster scan pattern is a square of 3×3 mm^2 and the substrate properties are associated with the bulk material for the entire substrate since the powders in previous layers have completely transformed from powders to solid. Figure 5 shows the comparisons of the simulated temperature contours and melt pools for the single straight scan and the multi-layer cross-raster scan simulations. The peak temperature of the raster scan is higher than that of the single scan by about 50 °C which is not remarkable. However, it is obvious that the high temperature penetration becomes much deeper, shown in the cross sectional view A-A for the raster scanning simulation, and it is noted that the raster scan does not have a very sharp melt pool tail as in the single straight scan, although the overall melt pool dimensions were similar to that obtained in the single scan.
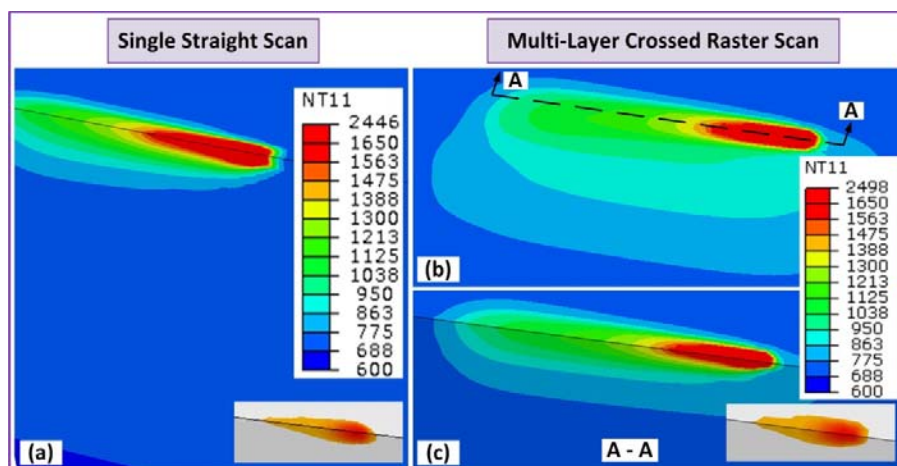

Figure 5. Comparisons of simulated temperature contours and melt pools for (a) the single straight scan and (b) the multi-layer cross-raster scan.
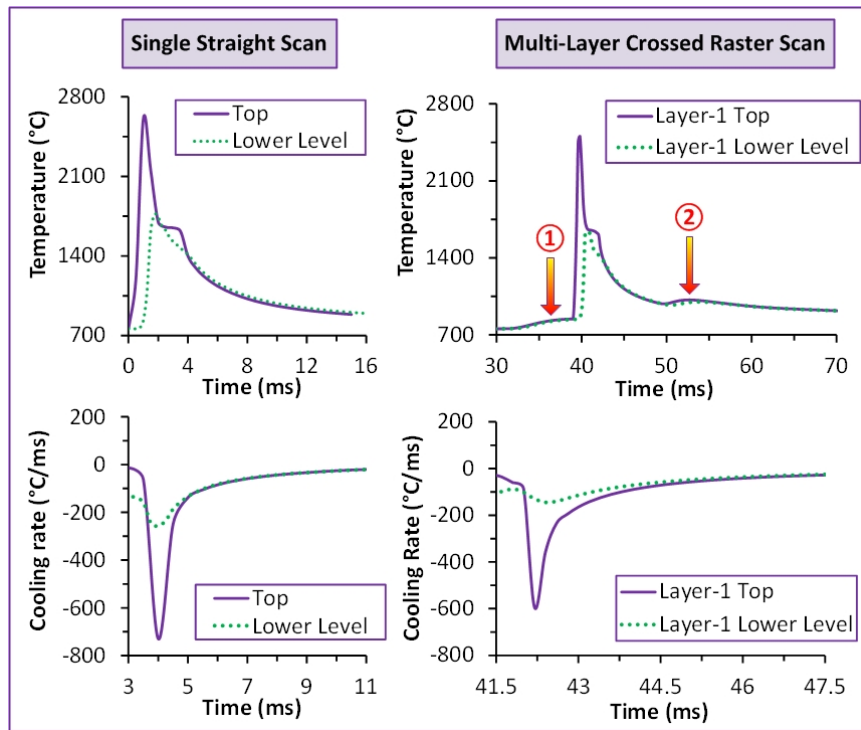
Figure 6. Comparisons of simulated temperature and cooling rate histories for the single straight scan and the multi-layer cross-raster scan.

Figure 6 illustrates the simulated temperature and cooling rate histories between the single straight scan and the raster scan. Both of the temperature and the cooling rate histories discussed in this part were obtained from two locations: (A) a nodule at the top surface and at the center of the melt pool at a certain time frame (labeled "Layer Top") and (B) the nodule just below this node on the bottom of the powder layer (labeled "Lower Level" or "Layer Bottom"). All the cooling rates discussed in this study are after the temperature generally drops below the liquidus temperature. Significant differences can be clearly noted that despite of the plateau (due to the latent heat of fusion), the simulation of the raster scan can capture the ramp denoted as ① due to the residual heat from the previous adjacent scans and the small bump denoted as ② due to the subsequent heating from the adjacent scans. These differences may apparently affect the resultant microstructures during material solidifications. The cooling rates from the raster scan are noticeably lower than those of the single scan simulation due to the lingering heat from the previous scans. Therefore, the analysis with a raster scan pattern may be necessary because of the difference in the melt pool geometry, temperature penetration, temperature history, and cooling history corresponding to those of the single straight scan simulation. All of them are generally due to the residual heat from the previous scans. Furthermore, as stated above, the multi-layer cross-raster scan analysis is required for the thermo-mechanical simulation because of residual thermal strains accumulated through the repeated layer-melting process.

Half-Solid, Half-Powder Substrate

This case study of the overhang geometry in a part was partially represented by a half-solid, half-powder substrate. Since the thermal phenomena have been discussed earlier, the focus

781

in this section is on the thermal behaviors in the individual portions, solid substrate vs. powder substrate, and the phenomena at the solid/powder substrate transition. In this study, the raster direction is perpendicular to the solid/powder substrate interface (S/P interface) in the first powder layer; the electron beam moves between the solid- and the powder-substrate back and forth. The raster direction is along the S/P interface in the second powder layer.
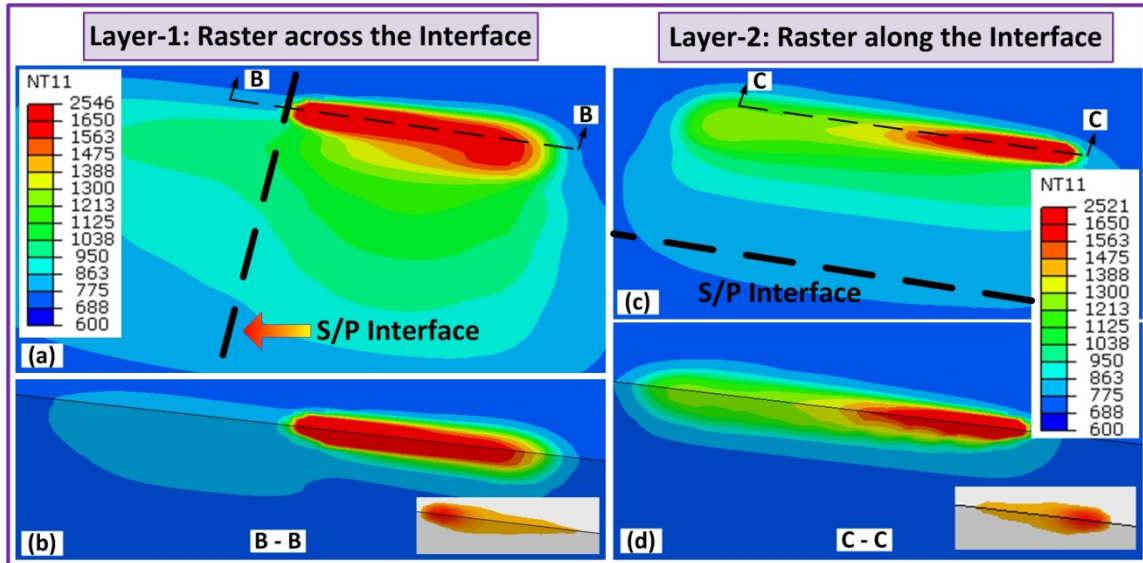

Figure 7. Comparisons of simulated temperature contours and melt pools for the layer of raster across/along the in solid/powder interface.

Figure 7 compares the simulated temperature contours and the melt pool sizes for the thermal analysis of two layers right at an overhang structure (again represented by half-solid, half-powder). The significant effect of the powder substrate can be clearly observed in Figure 7a and 7b; the residual heat in the powder layer in the powder-half is more prominently than that in the solid-half, especially at the top surface in Figure 7a, but the solid side has a much greater temperature penetration with an obvious step at the S/P interface shown in Figure 7b. Nevertheless, the peak temperatures do not seem to change significantly from the solid side to the powder side, by the increase within 100 °C. All the above phenomena are because of the much larger thermal resistance in the powder substrate, so that the heat is more likely to be dissipated in the solidified layer on the powder side other than along the penetration direction. For the same reason, the melt pool length is as long as 1.22 mm in the powder side in Layer-1 which is much longer than the 0.75 mm in the solid side. However, the melt pool length is 0.85 mm in the powder side in Layer-2 which is fairly shorter than expected, but the peak temperature is still at the same level as that in the powder side in Layer-1.

Conclusions

In this study, a developed FE thermal model for the EBAM process was extended to investigate the preheating process as the thermal initial conditions before the actual electron beam scanning and melting process. The model has also been improved to demonstrate its capability of multi-layer raster patter scanning. Moreover, a case study examining the powder effect on the thermal characteristics was analyzed. The major findings are summarized as follows.

- The preheating temperature penetration is about 0.5 mm with the critical substrate thickness of 10 mm beyond which the preheating temperature penetration will not be significantly affected.
- The modified FE thermal model that considers preheating as the initial condition, which is close to actual conditions, shows significant effects on the temperature results.
- The analysis with a raster scanning pattern may be necessary because of the difference in the melt pool geometry, temperature penetration, temperature history, and cooling history compared to a single straight scan simulation. All of them are generally due to the residual heat from previous scans. In addition, the multi-layer cross-raster scan simulation is required in the thermo-mechanical analysis.
- Due to the large thermal resistance in the powder substrate, more residual heat is confined in the powder layer in the powder substrate side and a stepped change in the temperature penetration at the S/P interface is very noticeable. For the same reason, the melt pool length can be as long as 1.22 mm in the powder side, which is much longer than the 0.75 mm in the solid side.
- Future investigations will include the thermo-mechanical aspect in the EBAM process for residual stress and part distortion predictions.

Acknowledgement

References

[1]   Heinl, P., Rottmair, A., Korner, C., and Singer, R. F., 2007, "Cellular titanium by selective electron beam melting," Advanced Engineering Materials, 9(5), pp. 360-364.
[2]   Gaytan, S. M., Murr, L. E., Medina, F., Martinez, E., Lopez, M. I., and Wicker, R. B., 2009, "Advanced metal powder based manufacturing of complex components by electron beam melting," Materials Technology, 24, pp. 180-190.
[3]   Available from: http://www.arcam.com/.
[4]   Zaeh, M. F., and Lutzmann, S., 2010, "Modelling and simulation of electron beam melting," Production Engeering. Research and Development, 4, pp. 15-23.
[5]   Shen, N., and Chou, Y. K., "Thermal modeling of electron beam additive manufacturing process - powder sintering effects," Proc. the 7th ASME 2012 International Manufacturing Science and Engineering Conference (MSEC2012).
[6]   Ferro, P., Zambon, A., and Bonollo, F., 2005, "Investigation of electron-beam welding in wrought Inconel 706—experimental and numerical analysis," Materials Science and Engineering: A, 392(1–2), pp. 94-105.
[7]   Liu, C., Wu, B., and Zhang, J., 2010, "Numerical Investigation of Residual Stress in Thick Titanium Alloy Plate Joined with Electron Beam Welding," Metallurgical and Materials Transactions B, 41(5), pp. 1129-1138.
[8]   Rouquette, S., Guo, J., and Le Masson, P., 2007, "Estimation of the parameters of a Gaussian heat source by the Levenberg-Marquardt method: Application to the electron beam welding," International Journal of Thermal Sciences, 46(2), pp. 128-138.

[9] Taylor, G. A., Hughes, M., Strusevich, N., and Pericleous, K., 2002, "Finite volume methods applied to the computational modelling of welding phenomena," Applied Mathematical Modelling, 26(2), pp. 311-322.

[10] De, A., and DebRoy, T., 2007, "Improving reliability of heat and fluid flow calculation during conduction mode laser spot welding by multivariable optimisation," Science and Technology of Welding and Joining, 11, pp. 143-153.

[11] Sih, S. S., and Barlow, J. W., 2004, "The prediction of the emissivity and thermal conductivity of powder beds," Particulate Science and Technology, 22, pp. 291-304.

[12] Tolochko, N. K., Arshinov, M. K., Gusarov, A. V., Titov, V. I., Laoui, T., and Froyen, L., 2003, "Mechanisms of selective laser sintering and heat transfer in Ti powder," Rapid Prototyping Journal, 9, pp. 314-326.

[13] Zhang, Y., and Chou, Y. K., 2006, "Three-dimensional Finite Element Analysis Simulations of the Fused Deposition Modelling process," Journal of Engineering Manufacture (Proceedings of the Institution of Mechanical Engineers Part B), 220(10), pp. 1663-1671.

[14] Zhang, Y., and Chou, Y. K., 2008, "A Parameter Study of Part distortions in FDM Using 3D FEA," Journal of Engineering Manufacture (Proceedings of the Institution of Mechanical Engineers Part B), 222, pp. 959-967.

[15] He, X., 2006, "Heat Transfer, Fluid Flow and Mass Transfer in Laser Welding of Stainless Steel With Small Length Scale," Doctor of Philosophy, Pennsylvania State University, University Park.